Optics and Lasers in Engineering 50 (2012) 210–214

Contents lists available at SciVerse ScienceDirect

Optics and Lasers in Engineering

journal homepage: www.elsevier.com/locate/optlaseng

Ultrafast laser machining of tapered microchannels in glass and PDMS

Samira Darvishi, Thomas Cubaud *, Jon P. Longtin

Department of Mechanical Engineering, Stony Brook University, Stony Brook, NY 11794-2300, USA

ARTICLE INFO

Article history:
Received 3 May 2011
Received in revised form
16 July 2011
Accepted 3 September 2011
Available online 28 September 2011

Keywords:
Femtosecond laser
Ablation
Fluence
Trenches
Microfluidics

ABSTRACT

The ability to fabricate tapered microchannels with customizable cross sections in a variety of materials is highly desirable for microfluidic applications. This article examines ultrafast laser machining of tapered microchannel trenches in both hard (soda–lime and borosilicate glasses) and soft (PDMS elastomer) transparent solids. A simple model for channel width and depth as a function of processing parameters and threshold fluence is presented. Estimated channel sizes from the model are in good agreement with experimental results. We also show that the channel depth is a linear function of the number of laser pulses per channel width. All measurement data are found to collapse onto a single curve, which can serve as a useful guide for micromachining of tapered channels in transparent materials.

1. Introduction

Small-scale flows are present in a wide range of fields [1–3], including biomedical diagnostics, cellular processes, environmental monitoring, control of micro-reactions, micro-power generation, and material synthesis [4–8]. The fabrication of microchannels in transparent media plays an important role for optofluidics elements of various shapes, such as cavities, fluid-reconfigurable lenses, and waveguides [9–11]. In particular, the controlled fabrication of tapered grooves or trenches at the small scale offers significant advantages for manipulating capillary flows and wetting phenomena in microgeometries [12]. Altering the topography of hydrophilic substrates with narrow Gaussian trenches may promote droplet adhesion due to the presence of large interfacial curvatures. In turn, such patterned surfaces find use in modifying the condensation and evaporation behavior of droplets. The cusped wedges demonstrated in this work, which differ from typical grooves having rectangular or triangular cross-sections [13], are also appealing for producing non-polygonal microfluidic channels. At the small scale, recent multiphase flow studies using high-viscosity fluids have highlighted the importance of the channel aspect ratio for initiating flow segregation and encapsulation processes [14,15].

There are still significant challenges in fabricating low-cost and reliable microfluidic modules in transparent media. Popular and lost-cost materials for microfluidic applications include glass, PMMA, and PDMS elastomer. Lithography techniques require advanced facilities and numerous process steps, and produce toxic waste. They are also often limited in both material choice and channel geometry. Embossing, injection molding, and similar thermoforming techniques, while providing excellent throughput and cost, are ineffective for rigid materials such as glass and are not suited for frequent changes to fluidic geometry [16–18].

Laser micromachining offers several advantages for fabricating microchannels, including the capability to form complex cross-sectional shapes that are beyond the reach of traditional lithographic techniques. A number of researchers have demonstrated forming channels in polymer materials using traditional laser processing, in which the laser is chosen to absorb strongly by the material to be machined [19–22]. The material removal occurs exclusively by thermal mechanisms, and the laser–material interaction is well defined by classical absorption and heating models. Straightforward models that predict channel geometry and dimensions have also been presented. For glass materials, a laser peeling technique has been reported using a CO_2 laser [23] in which a variety of channel cross-sections were formed, although the technique appears to be best suited for straight channels.

The use of *ultrafast lasers* (pulse duration <1 ps) for channel formation presents new opportunities for both material versatility and channel geometry. Ultrafast laser–material interactions and subsequent material removal are uniquely distinct from traditional thermal ablation in which materials normally transparent to the incident wavelength can be processed, and a non-linear mechanism is responsible for the laser–material energy coupling into the material. The material is ionized in the focal volume, and bonds are broken directly by the resulting electron–phonon interactions [24]. As a consequence the temperature rise and thermal diffusion in the surrounding material are negligibly small.

Bhuyan et al. present the fabrication of glass channels with minimal taper using a femtosecond laser [25]. Their approach,

* Corresponding author. Tel.: +1 631 632 9431; fax: +1 631 632 8544.
E-mail address: thomas.cubaud@stonybrook.edu (T. Cubaud).

0143-8166/$ - see front matter © 2011 Elsevier Ltd. All rights reserved.
doi:10.1016/j.optlaseng.2011.09.003

however, employed complex optics and beam shaping. In this article, the fabrication of tapered channels using an ultrafast laser system with a simple Gaussian beam profile and lens configuration is presented. This work examines the cross-sectional channel shape formed during femtosecond laser ablation of both hard and soft materials. Gaussian laser beams are well suited for the fabrication of tapered channels and are also readily available as the default beam profile in many laser systems. The materials are processed using a computer-controlled motion system while varying the workpiece speed, laser pulse energy, and number of passes. Optical microscopy is then used to characterize the resulting channel cross sections. For all of the materials in this study, it is found that the channel height versus the non-dimensional number of laser pulses per channel width falls onto a single curve.

The versatility of ultrafast laser micromachining of cusped trenches discussed in this article is attractive for the development of new microgeometries to probe the evolution of viscous-stratified flows. The narrow cusp at the bottom of the trenches can be used to trap liquid, e.g., to form surfaces that are difficult to dry, which could find use for lubrication, sensing, or micro-heat-pipe [26,27] applications.

2. Experimental setup

The experimental setup for laser micromachining of microfluidic channels is shown in Fig. 1. A Spectra-Physics SpitFire Pro amplifier femtosecond laser is used for all micromachining processes. This laser system has a nominal wavelength $\lambda=800$ nm, a nominal pulse duration of 120 fs, and a maximum energy of 2.1 mJ/pulse. The pulse repetition rate, f, is fixed by the manufacturer at 1000 Hz. The beam is horizontally polarized upon exiting the laser and the mode shape is nearly TEM_{00} with $M^2=1.3$.

The beam is directed to a 90° turning mirror followed by a waveplate-polarizing beam splitter for power attenuation. The attenuated beam is sent to a quartz plano–convex lens with focal length of $f_L=400$ mm. The sample is then located at the beam

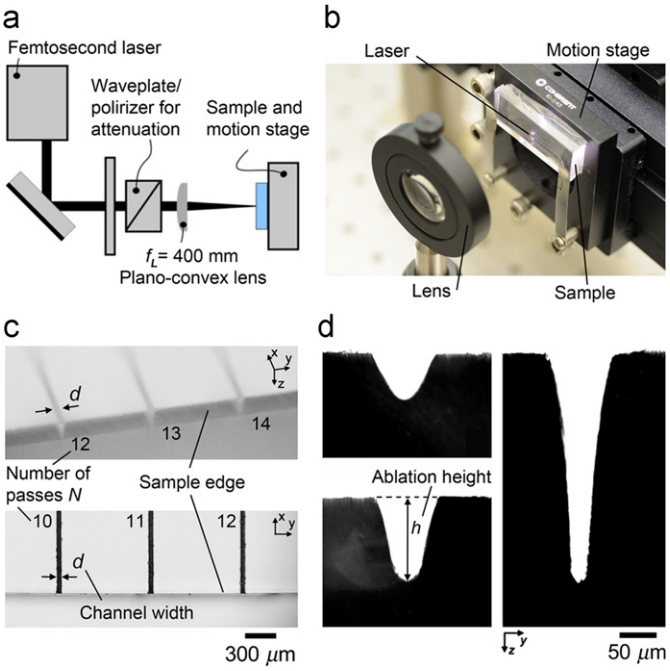

Fig. 1. (a) Schematic of the experimental setup for laser ablation, (b) photograph taken during the processing of a slab of polydimethylsiloxane (PDMS) elastomer, (c) micromachined of trenches with different numbers of passes N, and (d) micrographs of processed channels in borosilicate glass.

focal point, which is determined by locating the dull glow of the air breakdown at the focal point when the room is darkened. All power measurements are taken with a Molectron PD10 measurement head and AD500 display.

The incident beam radius a is calculated from the focal point using a knife-edge technique [28]. To minimize the edge ablation, the power is attenuated to 65 mW and a 0.5 mm mild steel rectangular plate is indexed across the beam as the beam block. The power versus, position locations are then fit to a standard Gaussian profile to calculate the $1/e^2$ beam diameter [28], $d_i=2a$. The beam diameter as measured from the knife-edge technique was $d_i=110\pm10$ μm. For comparison, the beam diameter estimated from the lens equation for a Gaussian beam is $d_i=4M^2f_L\lambda/(\pi D)=107$ μm, where $D=0.5$ cm is the spot size on the focusing lens, which is in good agreement with the measured diameter [29].

Unlike traditional thermal processing, where a laser wavelength is chosen such that the material naturally absorbs the laser beam strongly, both glass and PDMS are transparent at the ultrafast laser wavelength of 800 nm used in this work. Strong energy coupling from the laser occurs due to non-linear multi-photon absorption and avalanche ionization [24]; however a minimum threshold fluence for ablation [30,31], F_{th}, is required for these mechanisms to initiate. If the fluence is below F_{th} then no energy couples into the material, and no material removal occurs. The threshold fluence is determined by maximally attenuating the beam, then placing the sample at the beam focus, and gradually increasing the beam power in a darkened room until light emission from the plasma associated with breakdown is observed, after which the average laser power P_{th} is measured. The threshold fluence is then calculated as $F_{th}=2P_{th}/(\pi fa^2)$ [29], where P_{th} is the minimum measured laser power for ablation.

Three materials were used in this study: (a) borosilicate glass, (b) soda–lime glass, and (c) polydimethylsiloxane elastomer (PDMS). Both glasses were used in the form of rectangular plates. Conventional PDMS (Down Corning Sylgard 184) was mixed and cured for 24 h at room temperature before starting the experiment. For each test, the sample is located in a 3-axis linear positioning system (Coherent LabMotion) that moves the sample as needed and also controls the laser beam delivery. The upper surface of the sample is located at the beam waist, and the samples are oriented with their thin edge parallel to the laser beam (Fig. 1b). Initially the beam is located away from the sample edge, and the sample is set into motion at speed V in a direction perpendicular to the beam. The edge of the sample is then brought into the beam focal region and material ablation begins. In this fashion, there is always a complete channel cross section available for ablated material to escape, as opposed to initially drilling a hole and then translating the workpiece to form a channel. The sample continues to move at constant velocity, V, for several millimeters to form a channel. The beam path can be repeated N times to remove additional material to achieve a desired ablation depth h.

In this experiment, successive straight trenches are formed 1 mm apart for various numbers of passes N and stage velocity V (Fig. 1c). Processed substrates are then placed vertically on an inverted microscope to photograph the channel trench profile (Fig. 1d). A fiber optic bundle emits a collimated beam of white light nearly parallel to each trench, so that the glass substrate appears dark and the channel profile is clear on the micrographs. The channel surface roughness is estimated from the micrographs to be less than 5 μm and no channel rim bulges on the top surface were observed.

3. Channel width and beam diameter

The fluence of a Gaussian laser pulse is maximal at the beam centerline and decreases radially as one moves away from the

centerline with position, $F(r)=F_{max}\exp(-2r^2/a^2)$, where r is the radial distance from the beam centerline, and F_{max} is the maximum fluence, which occurs at $r=0$ (beam centerline) [28]. For a Gaussian beam profile the beam radius a is defined as the point where the peak irradiance decays to $(1/e)^2 \cdot F_{max}$. Also, material ablation of transparent materials with ultrafast lasers is well known to depend on a minimum threshold fluence F_{th} (J/cm^2) [24,30,31], below which no material is removed. These parameters are shown schematically in Fig. 2.

The width d of the trenches fabricated using an ultrafast incident laser beam can be estimated based on the threshold fluence. For a laser beam of radius a moving across the sample surface at speed V with a pulse repetition rate f, the distance between two adjacent pulses is V/f. When normalized by the incident beam radius a on the sample, the non-dimensional step size $\beta=V/fa$ represents the fraction of the beam radius that the beam moves between successive pulses. For a Gaussian pulse, the maximum fluence is delivered at the point on the sample directly under the centerline of the beam path, and decreases as one moves away from the centerline. For material to be removed with a given pulse, the fluence must be at least F_{th}. At any given point on the workpiece surface, the laser fluence increases with each pulse as the laser beam approaches the point, followed by decreasing fluence as the beam recedes away.

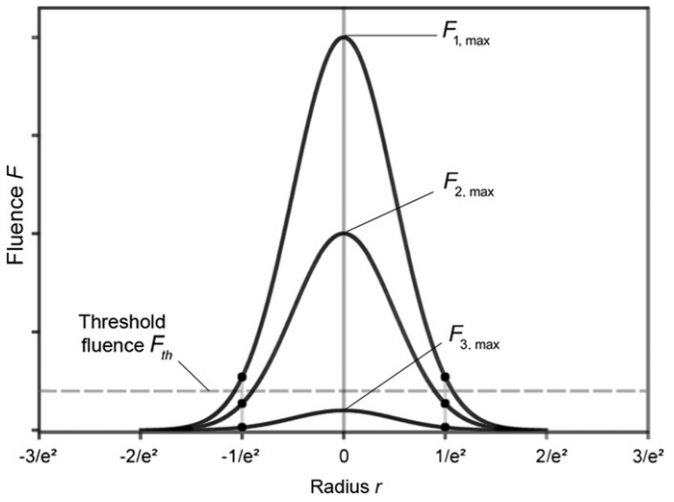

Fig. 2. Gaussian pulse profile and example of threshold fluence F_{th}. Optical $1/e^2$ beam diameter does not change with laser peak fluence (hence laser power or pulse energy). Laser fluence must exceed F_{th} for material to be removed, i.e., $F_{max}/F_{th} \geq 1$. Thus F_1 and F_2 will produce channels larger than and smaller than the $1/e^2$ beam diameter, respectively, while F_3 will not produce a channel at all because no part of the pulse exceeds F_{th}.

If the distance between pulses is small as compared to the beam radius, i.e., $\beta \ll 1$, then the 'scalloping' effect that occurs at the edges of the trenches is negligible and a simple analytical expression for the channel diameter can be obtained by determining the value of r for which material will be removed, i.e., $F \geq F_{th}$: $r \leq a[\ln(F_{max}/F_{th})/2]^{1/2}$. Two checks on the results can be made: First, if $F_{max}/F_{th} < 1$, no material will be removed, because no portion of the incident laser pulse would be large enough to exceed the breakdown threshold. Second, since the incident beam diameter $d_i=2a$ is defined as the diameter when the fluence drops to $(1/e^2) \cdot F_{max} \approx F_{max}/7$, one would expect the channel width to be on the order of the beam diameter, i.e., $d \sim d_i$ when $F_{max} \sim 7F_{th}$.

Note that in this model the amount of material removed is not considered. Estimates of material removal versus laser processing parameters could be included in the model using studies by other researchers of mass removal for ultrafast laser material interactions [30,31].

4. Results and discussion

The channel width d at the top of the trench and ablation depth h are systematically measured for different materials and operating conditions. The channel aspect ratio $\alpha=h/d$ can be readily altered with the laser speed V, power P, pulse frequency f, and number of passes N. We observe that d increases with the channel aspect ratio for $\alpha < 2$ and remains constant at a final diameter d_f for $\alpha > 2$ (Fig. 3a). The final channel diameter d_f is also a function of the incident laser power P (Fig. 3b). The threshold power for the ablation process is used to determine the threshold fluence. The measured threshold powers for borosilicate glass, soda-lime glass, and PDMS were 95, 75, and 55 mW, corresponding to F_{th}= 2.0, 1.8, and 1.2 J/cm^2 respectively. The values for the glasses agree reasonably well with values from the literature, e.g., 1.7 J/cm^2 for borosilicate glass [32].

Referring to Fig. 3c, for both glass materials $d \sim d_i$ for $F_{max} \sim 7F_{th}$ as predicted above. The width of the channel for PDMS, however,

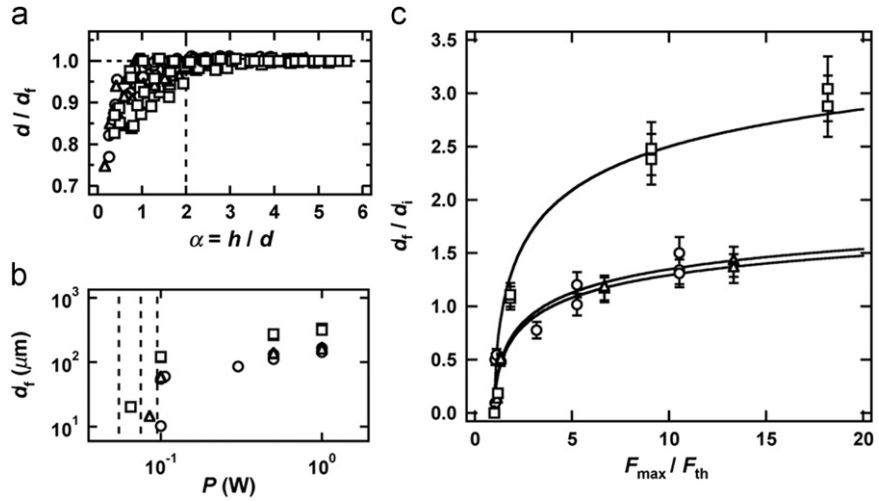

Fig. 3. Evolution of channel width d. Materials: borosilicate glass (○), soda–lime glass (△), and PDMS elastomer (□). (a) Influence of the channel aspect ratio $\alpha=h/d$, (b) final channel width d_f versus incident laser power P. Dashed-lines: threshold of ablation process, and (c) evolution of the final channel width d_f scaled by the incident laser beam diameter d_i as a function of the ratio of the maximum fluence F_{max} to the threshold fluence F_{th}. Solid lines: $d_f/d_i=g[\ln(F_{max}/F_{th})]^{1/2}$ with $g=0.88$ (borosilicate), 0.85 (soda-lime), and 1.65 (PDMS).

is several times greater than both predicted values and the measured values for the glass. This is particularly striking at the high fluence levels, where the channel width is nearly three times greater than the incident beam diameter. This result suggests that the flexibility (high compliance) of the PDMS material seems to factor strongly in the ablation and material removal mechanisms, as well as the final channel geometry. Further work is required to elucidate the mechanisms and key parameters that influence the channel width in PDMS and similar compliant materials.

The non-dimensional channel width d_f/d_i versus the non-dimensional fluence F_{max}/F_{th} is fit using the function $d_f/d_i = g[\ln(F_{max}/F_{th})]^{1/2}$ introduced in the previous section, and good agreement with experimental data is found with $g=0.88$ for borosilicate, $g=0.85$ for soda-lime, and $g=1.65$ for PDMS elastomer (Fig. 3c). For the PDMS case, the effective channel width d_f used in the model is extrapolated from the general trench profile. Overall, the channel width is reasonably well predicted by the model over the fluence range of interest.

To assess the evolution of the depth of the channels versus number of passes N, the edge of the trench is extracted using image processing after each pass, with successive passes superposed onto a composite image to study the influence of N while keeping the other parameters constant, as shown in Fig. 4. It is evident from these figures that the channel width d reaches its saturation value d_f quickly, after $N\sim2$–3 for $\alpha>2$ similar to Fig. 3a. In contrast, the ablation height h changes dramatically with increasing N. The channel profiles in glasses (borosilicate and soda-lime) have a narrow "V" shape that is mildly convex for $\alpha \gg 1$, and are well fit using a Gaussian function, i.e., the laser beam literally leaves its intensity footprint carved into the glass.

For the silicone elastomer (PDMS) in Fig. 4c, however, the channel cross section remains nearly constant after the initial channel width is established after 3–4 pulses, with only a gradual tapering with depth, even for $\alpha \gg 1$. (Note that the glass and PDMS images do not share the same scale; the PDMS channels are nearly 4× wider and deeper as evident from the reference scales). One possible explanation is that the PDMS, being very flexible, deforms substantially during the material removal phase, with the result that the edges of the channel simply deform, rather than resisting and being ablated. Ultrafast lasers are capable of generating very large pressure waves due to the fact that the energy deposition and heating occur in the focal volume at a time scale much faster than that based on the speed of sound [33,34], unlike long-pulse lasers in which the acoustic transient propagates away during the heating process. As a result, for ultrafast lasers a very large pressure wave is produced both in the solid material and the plume of ejected material above the sample. Further work is needed to clarify the nature of the channel shape for PDMS.

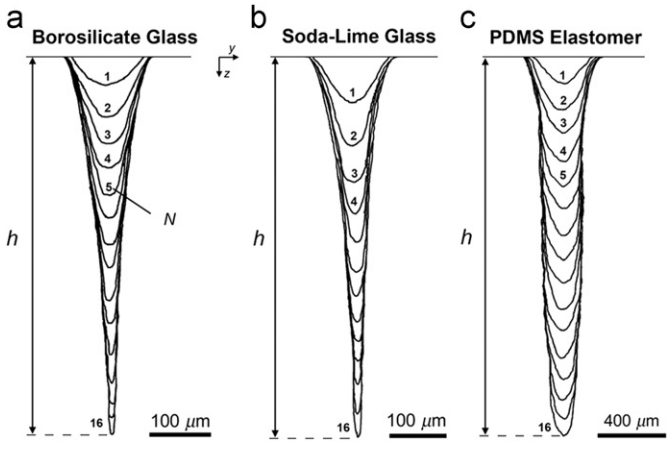

Fig. 4. Influence of the number of passes N on microtrenches profiles: (a) borosilicate glass, (b) soda–lime glass, and (c) PDMS elastomer.

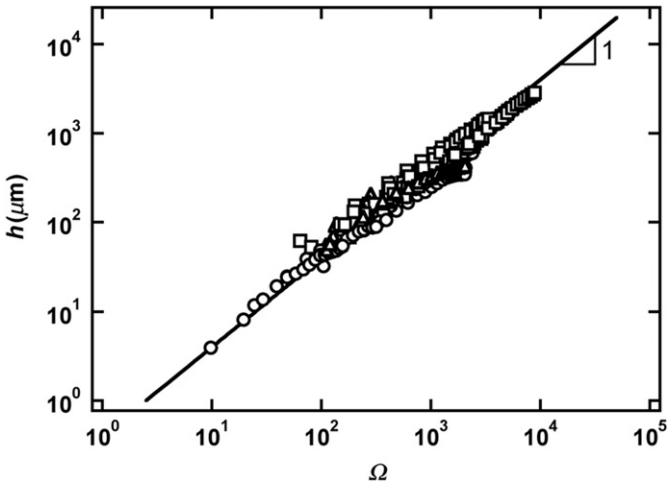

Fig. 5. Evolution of the channel height h versus number of laser pulses per channel width $\Omega=Ndf/V$ with materials: borosilicate glass (○), soda-lime glass (△), and PDMS elastomer (□). Low and large aspect ratios (i.e., $\alpha<2$ and $\alpha>12$) are not displayed. Solid line: $h=0.4\Omega$.

Next attention is turned to the ablation height h. An important parameter for laser ablation techniques is the number of laser pulses associated with the formation of a feature [35,36]. In our system, since the beam is moving with a velocity V, we define the number of pulses per channel diameter as $\Omega=Ndf/V$. This parameter allows for rescaling of all measurement data for both glasses and PDMS, including displacement speed V (ranging between 0.5 and 5 mm s^{-1}), effective channel width d, number of passes N (ranging between 1 and 16), and laser frequency $f=1$ kHz, onto a single master curve for a channel aspect ratio α ranging between 2 and 12. The results are shown in Fig. 5. This curve is fit with the function $h=c\Omega$, where $c=0.4$ μm/pulse.

For $\alpha>15$, the curve overestimates the ablation penetration depth h into the material, as in practice h asymptotically reaches a plateau around $\alpha\approx15$. Studies of deep-hole drilling have shown that the maximum h is essentially limited by the rate of ejection of the ablated material trapped within the structure [35,36]. However, laser fabrication of *channels* is distinct from drilling *holes*. In the former case the ablated material can escape from the side of the channel, whereas the only means of material removal during drilling is for the material to pass back up the entire length of the hole [35,37]. The much larger exit area available when fabricating channels is a plausible explanation for the increased values of h found in channel fabrication. Also, at the opposite extreme, the ability to fabricate very small channels should be possible since, in principle, small Ω should allow for etching of sub-micron-size channel depths, which may enable manufacturing of glass nanofluidic modules. Further work is required to explore this channel fabrication regime.

5. Conclusions

This article characterizes the impact of key processing parameters during ultrafast laser micromaching of microchannels fabricated in both glass and a soft polymer material (PDMS). Tapered channels are fabricated using an ultrafast laser with wavelength of 800 nm and a Gaussian beam profile focused onto the sample surface. The sample speed, number of passes, and laser power are varied, after which an optical microscope is used

to assess the channel cross-sectional geometry and dimensions. A simple model based on the total delivered fluence and ablation threshold associated with ultrafast laser micromachining provides a reasonably good estimate of the final channel width as a function of laser processing parameters for glass materials. A single parameter that captures the number of pulse per channel diameter is introduced and allows for rescaling all of the experimental data onto a single master curve across four orders of magnitude. The resulting curves provide the key parameters and functional relationships for advanced laser micromachining of tapered microchannels. The PDMS material differs notably in several respects from the glass, including significantly larger channel widths and a stronger dependence of the width on incident laser power. Further work is needed to characterize and explain the anomalously large channel widths and strong dependence on laser power in PDMS, and investigate the relationship between channel geometry and processing parameters in general for non-Gaussian laser beam profiles.

Acknowledgemnts

Funding for this work was provided in part by the National Science Foundation (CBET-0932925).

References

[1] Günther A, Jensen KF. Multiphase microfluidic: from flow characteristics to chemical and material synthesis. Lab Chip 2006;6:1487.
[2] Teh SY, Lin R, Hung LH, Lee AP. Droplet microfluidics. Lab Chip 2008;8:198.
[3] Song H, Chen DL, Ismagilov RF. Reactions in droplets in microfluidic channels. Angew Chem Int Ed 2006;45:7336.
[4] Craighead H. Future lab-on-chip technologies for interogating individual molecules. Nature (London) 2006;442:387.
[5] El-Ali J, Sorger PK, Jensen KF. Cells on chips. Nature (London) 2006;442:403.
[6] Yager P, Edwards T, GFu E, Helton K, Nelson K, Tam MR, et al. Microfluidic diagnostic technologies for global public health. Nature (London) 2006; 442:412.
[7] deMello AJ. Control and detection of chemical reactions in microfluidic systems. Nature (London) 2006;442:394.
[8] Meng DD, Cubaud T, Ho C-M, Kim C-J. A methanol-tolerant gas-venting microchannel for microdirect methanol fuel cell. J. Microelectromech. Syst. 2007;16:1403.
[9] Wolfe DB, et al. Dynamic control of liquid-core/liquid-cladding optical waveguides. Proc. Natl. Acad. Sci 2004;101:12434.
[10] Mao X, Waldeisen JR, Juluri BK, Huang TH. Hydrodynamically tunable optofluidic cylindrical microlens. Lab Chip 2007;7:1303.
[11] Tang SKY, Stan CA, Whitesides GM. Dynamically reconfigurable liquid-core liquid-cladding lens in a microfluidic channel. Lab Chip 2008;8:394.
[12] Herminghaus S, Brinkmann M, Seemann R. Wetting and dewetting of complex surface geometries. Ann Rev Mater Res. 2008;38:101.
[13] Madou MJ. Fundamental of microfabrication: the science of miniaturization. Boca Raton: CRC Press; 2002.
[14] Cubaud T, Mason TG. Formation of miscible fluid microstructures by hydrodynamic focusing in plane geometries. Phys Rev E 2008:78.
[15] Darvishi S, Cubaud T. Lubrication of highly viscous core-annular flows in microfluidic chambers. J Fluids Eng. 2011;133:031203.
[16] Becker H, Gartner C. Polymer microfabrication technologies for microfluidic systems. Anal Bioanal Chem 2008;390:89.
[17] Attia UM, Alcock JR. Integration of functionality into polymer-based microfluidic devices produced by high-volume micro-moulding techniques. Int J Adv Manuf Technol 2010;48:973.
[18] Eusner T, Hale M, Hardt DE. Process robustness of hot embossing microfluidic devices. J. Manuf. Sci. Eng-T A 2010:132.
[19] Snakenborg D, Klank H, Kutter JP. Microstructure fabrication with a CO_2 laser system. J. Micromech. Microeng. 2004;14:182.
[20] Romoli L, Tantussi G, Dini G. Layered laser vaporization of PMMA manufacturing 3D mould cavities. CIRP Ann—Manuf. Technol. 2007;56:209.
[21] Romoli L, Tantussi G, Dini G. Experimental approach to the laser machining of PMMA substrates for the fabrication of microfluidic devices. Opt Lasers Eng 2011;49:419.
[22] Nayak NC, Lam YC, Yue CY, Sinha AT. CO_2-laser micromachining of PMMA: the effect of polymer molecular weight. J. Micromech. Microeng. 2008:18.
[23] Zheng HY, Lee T. Studies of CO_2 laser peeling of glass substrates. J. Micromech. Microeng. 2005;15:2093.
[24] Gattass RR, Mazur E. Femtosecond laser micromachining in transparent materials. Nat Photon 2008;2:219.
[25] Bhuyan MK, Courvoisier F, Lacourt PA, Jacquot M, Furfaro L, Withford MJ, et al. High aspect ratio taper-free microchannel fabrication using femtosecond Bessel beams. Opt Express 2010;18:566.
[26] Longtin JP, Badran B, Gerner FMA. One-dimensional model of a micro-heat pipe during steady- state operation. J Heat Trans.-Trans A 1994;116:709.
[27] Bai PF, Tang Y, Tang BA, Lu LS. Thermal performance of heat pipe with different micro-groove structures. J. Cent South Univ Technol 2008;15:240.
[28] Khosrofian JM, Garetz BA. Measurement of a Gaussian laser-beam diameter through the direct inversion of knife-edge data. Appl Opt. 1983;22:3406.
[29] Siegman AE. Lasers. Sausalito: University Science Books; 1986.
[30] Perry MD, Stuart BC, Banks PS, Feit MD, Yanovsky V, Rubenchik AM. Ultrashort-pulse laser machining of dielectric materials. J. Appl. Phys. 1999;85:6803.
[31] Stuart BC, Feit MD, Rubenchik AM, Shore BW, Perry MD. Laser-induced damage in dielectrics with nanosecond to subpicosecond pulses. Phys. Rev. Lett. 1995;74:2248.
[32] Ben-Yakar A, Byer RL. Femtosecond laser ablation properties of borosilicate glass. J. Appl. Phys. 2004;96:5316.
[33] Sakakura M, Terazima M. Initial temporal and spatial changes of the refractive index induced by focused femtosecond pulsed laser irradiation inside a glass. Phys Rev B 2005:71.
[34] Sakakura M, Terazima M, Shimotsuma Y, Miura K, Hirao K. Observation of pressure wave generated by focusing a femtosecond laser pulse inside a glass. Opt Express 2007;15:5674.
[35] Shah L, Tawney J, Richardson M, Richardson K. Femtosecond laser deep hole drilling of silicate glasses in air. Appl Surf Sci 2001;183:151.
[36] Shah L, Tawney J, Richardson M, Richardson K. Self-focusing during femtosecond micromachining of silicate glasses. IEEE J Quantum Electron 2004; 40:57.
[37] Efimov OM, Glebov LB, Grantham S, Richardson M. Photoionization of silicate glasses exposed to IR femtosecond pulses. J. Non-Cryst Solids 1999;253:58.